

# PROCEEDINGS OF SPIE

[SPIDigitalLibrary.org/conference-proceedings-of-spie](https://spiedigitallibrary.org/conference-proceedings-of-spie)

## Quantum dot photoconductive antenna-based compact setups for terahertz spectroscopy and imaging

Gorodetsky, Andrei, Yadav, Amit, Smirnov, Semyon, Bazieva, Natalia, Rafailov, Edik

Andrei Gorodetsky, Amit Yadav, Semyon V. Smirnov, Natalia Bazieva, Edik U. Rafailov, "Quantum dot photoconductive antenna-based compact setups for terahertz spectroscopy and imaging," Proc. SPIE 11499, Terahertz Emitters, Receivers, and Applications XI, 1149905 (20 August 2020); doi: 10.1117/12.2567630

**SPIE.**

Event: SPIE Optical Engineering + Applications, 2020, Online Only

# Quantum dot photoconductive antenna based compact setups for terahertz spectroscopy and imaging

Andrei Gorodetsky<sup>1,2</sup>, Amit Yadav<sup>3</sup>, Semyon V. Smirnov<sup>3</sup>, Natalia Bazieva<sup>3</sup>, and Edik U. Rafailov<sup>3</sup>

<sup>1</sup>School of Physics and Astronomy, University of Birmingham, Birmingham B15 2TT, UK

<sup>2</sup>ITMO University, St. Petersburg 197101, Russia

<sup>3</sup>Aston University, Birmingham B4 7ET, UK

## ABSTRACT

We present the overview of the results on the development of compact THz setups based on the quantum dot photoconductive antennas obtained during the past five years. We demonstrate the potential of the InAs/GaAs Quantum-Dot based setups to become an efficient approach to compact, room-temperature operating CW and pulsed terahertz setups for spectroscopy and imaging. We describe the photoelectronic processes in quantum dot substrates and reveal the role of quantum dots in free carrier lifetimes and the formation of the ultrafast photocurrent. We demonstrate the operation mode of the proposed antennas in pulsed and CW regimes under resonant (carriers are excited only inside the quantum dots) and off-resonant (carriers are excited in the bulk volume of the substrate) pumps with compact quantum dot semiconductor lasers. The results allow suggesting the quantum dot based setups as a new approach to field condition compact THz sources for imaging and spectroscopy.

**Keywords:** photoconductive antennas, quantum dot lasers, compact THz setups, THz imaging, THz spectroscopy

## 1. INTRODUCTION

Terahertz (THz) frequency band of the electro-magnetic spectrum, usually defined to occupy frequencies between 100 GHz and 10 THz (30–3000  $\mu\text{m}$ , 0.4–40 meV, 3.33–333  $\text{cm}^{-1}$ ), is situated between microwave and infrared radiation. In contrast to the latter, the THz radiation, despite the fact that it was first obtained at the beginning of the XX century,<sup>1</sup> until relatively recently ( $\sim$  90s of the XX century) remained virtually unexplored, being even often referred to as 'gap',<sup>2</sup> and the amount of knowledge and technology associated with it is still very much inferior to the technologies associated with radiation in neighbouring ranges. This is primarily due to the lack of both sources of sufficiently powerful controlled terahertz radiation and receivers capable of accurately analysing and recording information about the radiation of this spectral band.

At the same time, in this region of the spectrum lie the frequencies of elementary intraband excitations of semiconductors and dielectrics, vibrational and rotational spectra of polymers and biological molecules, including potentially hazardous substances, foodstuffs and medicines. Wavelength and pulse duration are small enough to allow the use of THz radiation for the study of ultra-fast processes in semiconductor and other materials, imaging, diagnosis of certain diseases, quality control of microcircuits, detection of biological and chemical agents. Another rapidly developing area of application for THz radiation is near- and mid-range wireless systems, as THz waves can provide broadband, noise-resistant data transmission.

The first sources of THz (then not yet designated as a separate range, but belonging to the far infrared radiation) were gas lasers, such as water vapor lasers,<sup>3</sup> but they were difficult to handle, unstable and bulky. As a result of scientific research over the past 30 years, several major approaches to generating THz radiation have emerged. Among them, the following directions can be distinguished: i) upconversion of microwave radiation, ii) generation of difference frequency or pulse envelope of optical or infrared pumping,<sup>4</sup> iii) direct generation

---

Further author information: (Send correspondence to A.G.)

A.G.: E-mail: andrei@itmo.ru

of THz radiation in quantum cascade lasers (QCLs) and iv) generation by accelerated carriers in free electron lasers (FELs).<sup>5</sup> The latter, despite their maximum power and tunability, are unlikely to ever exceed the limits of scientific centers. THz QCLs, despite significant progress in the past few years, and elevated efficiency, do not yet allow reaching generation below 2 THz, and still require cryogenic cooling for efficient operation,<sup>6</sup> and, therefore, can also be used only in the laboratory environment.<sup>7</sup> Microwave avalanche diodes and Gunn diodes operate very efficiently at frequencies from 10 to 300 GHz, but with frequency increase up to and beyond 1 THz their efficiency drops very quickly.<sup>8</sup> Thus, especially for spectroscopy and ultra-fast process studies, pulsed and continuous wave optically pumped sources are of most interest.

Among the methods involving frequency downconversion the approach using intracavity mixing of infrared QCL radiation ( $\lambda = 9 - 10 \mu\text{m}$ ) in quantum well waveguides providing extremely high nonlinearity<sup>9</sup> looks very promising. Such devices are really compact (single chip), work at room temperature and allow for some tunability of the generated wavelength. However, strong absorption of THz radiation in waveguides, especially in the low-frequency region of the spectrum, limits their efficiency below 3 THz. Among the remaining methods one can mention the generation in plasma formed by the focused femtosecond laser beam from the amplifier<sup>10</sup> as the most scalable in power, but it can be implemented only in laboratory conditions and requires significant resources. Generation in nonlinear crystals, although it allows obtaining quasi-monochromatic THz radiation of higher powers, has the same drawbacks as generation in plasma, so the most promising from the practical applications point of view, i.e. THz spectroscopy and imaging with radiation of a particularly interesting spectral region from 0.3 to 3 THz are photoconducting antennas.<sup>11</sup> They are compact, do not require high pump powers and have a very high conversion factor of the optical pumping energy into THz, exceeding the limitations imposed by the Manley-Rowe ratio, due to the voltage applied to the antenna electrodes. Despite some reasonable progress made by various scientific groups in the last five years, the optimal solution to improve the efficiency of generating both broadband pulse and tunable continuous THz radiation while maintaining a compact size of the setup and operation at room temperature is still relevant and timely area of research.

The main obstacles to the widespread use of photoconductive antennas (PCAs) until recently, were the limited range of usable optical pump wavelengths ( $\lambda \leq 850 \text{ nm}$ ) to match the bandgap of commonly used low-temperature gallium arsenide (LT-GaAs) substrates, and their thermal instability due to a large number of defects. At the same time, the presence of such defects is necessary, as they serve as free carrier capture sites, for achieving subpicosecond lifetimes, essential for efficient and broadband PCA operation, especially in CW regime. The third limiting factor is the low absorption factor of laser pump radiation in the antenna gap, and low carrier concentration in semiconductor surface layer. This work addresses all these limitations and suggests the ways to overcome them.

The main scope of this work is the development of compact efficient and tunable room temperature operating transceivers of pulsed and CW THz radiation by the use of quantum dot (QD) based substrates.<sup>12</sup> Despite a great worldwide interest in the past 5-7 years, and significant progress made, nowadays there are still no optimal ultimate solution for compact THz spectroscopic and/or imaging setup based on the new compact efficient room-temperature sources, and results obtained here, may lay the basis for its further development.

## 2. QUANTUM DOT PHOTOCONDUCTIVE ANTENNAS

First QD materials were obtained at approximately the same time,<sup>13,14</sup> with the first generation of THz PCAs.<sup>15</sup> Quantum dots are often called "hand-made atoms"<sup>16</sup> because they have discrete energy levels that depend not so much on the material they are made of, but rather on their size. Photoelectronic properties of quantum dots can be controlled by changing their size during growth. The nanometer size of the QDs means that the quantum-dimensional effect is shown in all three dimensions, in contrast to the semiconductor quantum wells (QW), where the effect is present in only one dimension.

Optoelectronic materials for THz applications typically operate at pump wavelengths  $\lambda_{pump} \leq 850 \text{ nm}$  (LT-GaAs) or  $\lambda_{pump} \leq 1080 \text{ nm}$  (LT GaBiAs). For wavelengths  $1040 \leq \lambda_{pump} \leq 1300 \text{ nm}$ , on which InAs/GaAs QD semiconductor lasers usually operate, it is necessary to develop heterostructural materials, in particular, materials containing QDs, similar to those that can be found in such lasers.

Studies of effective ultrafast photoconducting materials for THz applications has already led researchers to the use of QD substrates,<sup>17-19</sup> where the main function of the layers with implanted QDs was to capture carriers and reduce their lifetime,<sup>17,20,21</sup> while pumping was performed at energies exceeding the width of the GaAs bandgap ( $\lambda_{pump} \leq 850$  nm). Indeed, lifetimes are an important parameter responsible for the spectrum width and THz generation efficiency.<sup>22</sup> Another important parameter is the mobility of charges, and it is significantly higher in QD substrates than in low-temperature grown semiconductors, due to lower concentration of defects. On the one hand, this is an advantage, as one can achieve large currents in the PCA, on the other hand, high mobility leads to higher dark currents, and since the efficiency of generating both continuous and pulsed THz radiation in a semiconductor is proportional to the current derivative, it is desirable to maximize the dark resistance values. The table 1 compares the material parameters for generating THz.

Table 1: Materials for PCA substrate

Material	pump Wavelengths	carrier lifetimes	Mobility	Ref.
SI GaAs	$\leq 850$ nm	$10^{-8} - 10^{-9}$ s	$5 - 10 \times 10^3$ cm <sup>2</sup> / s	<sup>23</sup>
LT-GaAs	$\leq 850$ nm	$10^{-12} - 10^{-13}$ s	$1 - 3 \times 10^3$ cm <sup>2</sup> / s	<sup>23</sup>
LT-GaBiAs	$\leq 1150$ nm	$10^{-11} - 10^{-12}$ s	$4 - 8 \times 10^3$ cm <sup>2</sup> / s	<sup>24,25</sup>
InAs/GaAs QD	$\leq 850$ nm, $1000 \leq 1300$ nm	$10^{-11} - 10^{-12}$ s	$3 - 7 \times 10^3$ cm <sup>2</sup> / s	<sup>20,26,27</sup>

Thus, QD materials have all the characteristics necessary for efficient generation of THz radiation in the PCA, and having grasped this premise, we proceed to their consideration.

For the purpose of THz generation, several InAs/GaAs QD structures containing different numbers of InAs QD layers within a GaAs lattice were grown. Their ground states (GS) were pre-calculated to correspond to the wavelength of ultrafast semiconductor lasers available at the time of production. The structures were grown over a 30-layer distributed Bragg reflector (DBR), which was pre-calculated to match the very same wavelength ( $\sim 1250$  nm). All semiconductor structures were grown by molecular beam epitaxy (MBE) in the Stranski-Krastanow regime, comprising a 30 nm top layer of LT-GaAs above an active region. The top layer of LT-GaAs significantly reduces the device dark current, yet comprises a very low fraction of active region volume and is optically transparent at longer optical pump wavelengths ( $\geq 870$  nm).

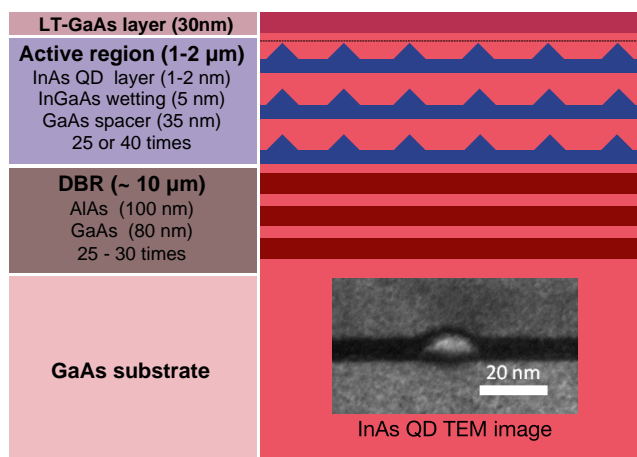


Figure 1. General layout of the QD substrate used for THz generation and TEM image of a single InAs QD

Individual QD layers were capped by 4–5 nm In<sub>0.15</sub>Ga<sub>0.85</sub>As layer and separated by a 35–36 nm GaAs spacer layer, giving a total active region depth between 1 μm and 1.7 μm for twenty-five to forty 40 nm QD sections.

Atomic force microscopy measurements of uncapped QD layers grown under similar conditions show a QD density of  $3 \times 10^{10} \text{ cm}^{-2}$  per layer, similar to areal QD densities for typical QD lasers. The fabrication of a metallic antenna over a semiconductor substrate was done using a standard UV photolithography and wet etching of the surface Ni/Au (40 nm/200 nm, respectively) features.

A layout of a QD substrate and a TEM image of a single QD are shown in Figure 1.

### 3. RESONANT OPERATION OF QUANTUM DOT BASED PHOTOCONDUCTIVE ANTENNAS

In this section, we review the results of THz generation in QD PCA pumped by the laser radiation with photon energy corresponding to the absorption bands of the implanted QDs, i.e. wavelength of 1100 nm to 1300 nm. Such wavelengths can be achieved in CW and ultrafast pulsed regimes by extremely compact and efficient QD semiconductor lasers.<sup>28</sup>

Picosecond and subpicosecond pulse durations, the ability to generate radiation at two wavelengths simultaneously, room temperature operation with passive cooling, and overall compactness make it possible to forecast the shiny prospects for QD lasers as pump sources for the QD PCA for effective generation of THz radiation.

#### 3.1 Generation and detection of pulsed THz radiation in quantum dot based photoconductive antennas under resonant pump.

The experimental system for testing of the QD-based PCA THz generation capability spectral response required broad wavelength tunability, which was achieved by using an optical parametrical oscillator (OPO). An amplified Yb:KGW laser system (Light Conversion "PHAROS") operating at 1030 nm wavelength with a pulse duration of 160 fs and repetition rate of 200 kHz was the main optical pump source. This laser was also used to drive a cavity-tuned optical parametric oscillator (OPO, Light Conversion "ORPHEUS") generating 160 fs duration pulses with a peak wavelength tunable between 640 nm to 2600 nm, and the THz output signal was detected by a sample of pre-characterised LT-GaBiAs PCA pumped with a Yb:KGW beam. The setup is shown in Figure 2 (a).

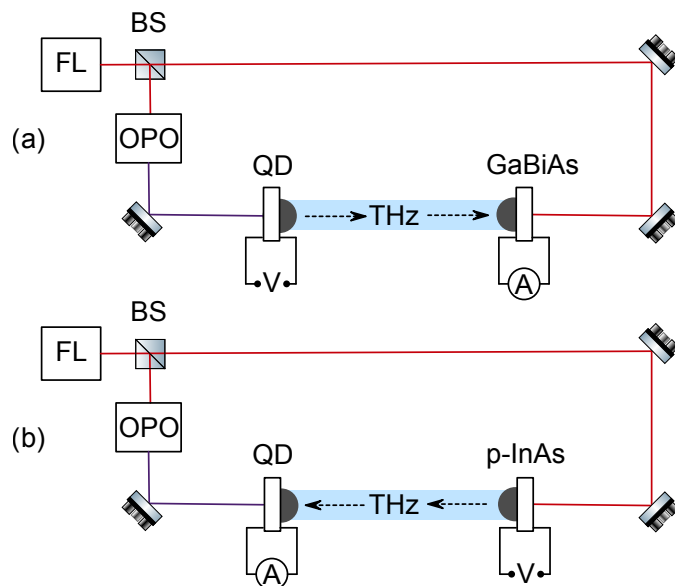


Figure 2. Experimental setup for testing of the QD-based PCA pump spectral response

To test the QDPCA operation as detector, biased pInAs PCA pumped with Yb:KGW beam was used as a THz source, and the dependence of the photocurrent in the QDPCA on pump wavelength was recorded (Figure 2 (b)). A dipole antenna with a length of  $\sim 90 \mu\text{m}$  and a PC gap width of  $\sim 10 \mu\text{m}$  was integrated with

QD-based structure in this experiment. Measured dependences of the photocurrents in emitter and detector regimes are presented in Figure 3.

The wavelength dependences of maximum photocurrent obtained both in the first experiment (QD PCA as emitter, GaBiAs PCA as detector, plotted with blue) and the second experiment (p-InAs PCA as emitter, QD PCA as detector, plotted with red), show the capability of the QDPCA to generate and detect pulsed THz radiation under  $\lambda = 1100\text{--}1300$  nm laser pumps,<sup>29</sup> as initial assumptions suggested. Secondly, these curves reveal distinct peaks in the vicinity of the intra-dot electron transitions corresponding to the QDs' first and second excited states (ES). Hence, QD based antennas may indeed be used in conjunction with semiconductor laser pump sources in the 1100–1300 nm wavelength range. However, although PL is strong at QD GS, neither THz generation nor detection was observed under pumping at these energy. To explain this, an additional study required, and the results are presented in section 3.2.

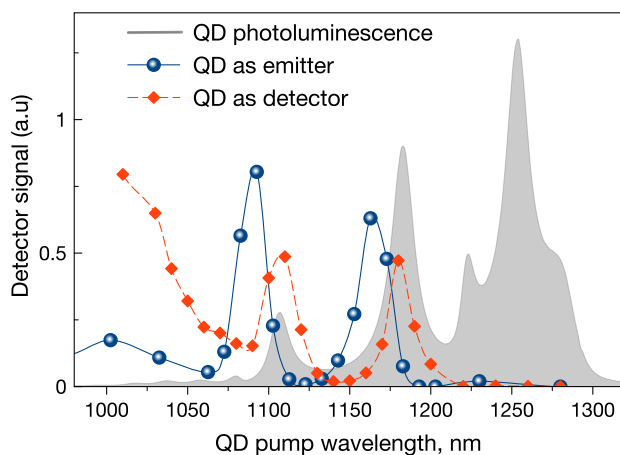


Figure 3. Efficiency of QDPCA as emitter (blue) and detector (red) superimposed on QD wafer photoluminescence (grey)

In 2019, an extremely high efficiency of THz generation in a PCA on a GaAs substrate with ErAs QDs was demonstrated.<sup>30,31</sup> The authors explain the observed pulse shape and extremely high conversion rate ( $\sim 0.2\%$ ) in the structure by the phenomenon of superradiation,<sup>32</sup> generated by the QD ensemble. Thus, an increase in the quality of QD substrates, namely the uniformity of QD sizes and their spacing can also lead to a further significant increase in the conversion of optical pump into THz radiation.

Efficient THz generation and detection under pump wavelengths shorter than  $\leq 870$  nm are due to carriers that were generated in the bulk GaAs lattice and captured by the QDs, showing the possibility to pump QDPCAs with a Ti:Sapphire fs laser. This regime and will be studied in detail in section 4.2.

### 3.2 Photocurrent in quantum dot substrates under resonant pump

To have deeper insights into the photoconductivity of the QD substrate under resonant pump, the temperature dependence of I-V curves under tunable laser pump was studied. The experimental setup layout for this experiment is shown in Fig. 4.

The pump source consisted of an InAs/GaAs QD laser diode with an active region containing 10 non-identical layers of InAs QDs. The laser was set up in a quasi-Littrow configuration. In this configuration, the radiation emitted from the back facet of the laser chip was collected with an AR-coated 40x aspheric lens (numerical aperture of 0.55) and coupled onto a diffraction grating (1200 grooves/mm), which reflected the first order diffraction beams back to the laser chip to provide the feedback. Wavelength tuning was achieved by rotating the diffraction grating. The laser output was monitored using an optical spectral analyser and a power meter. The laser maintained a broad tunability between 1140 nm to 1250 nm and a maximum output power of 435 mW.

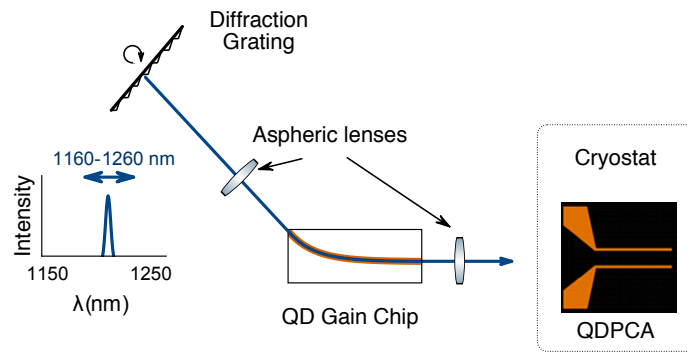


Figure 4. Setup for studying the photoconductivity of the QDPCA

To investigate the photoconductivity of the QD antenna at temperatures ranging from 13 K to 400 K under high vacuum ( $\sim 10^{-7}$  torr), the antenna was mounted on a copper holder inside a cryostat. A DC voltage sweep from  $-20$  V to  $+20$  V corresponding to the field values of  $-4$  kV/cm to  $+4$  kV/cm inside the antenna gap was applied. PCA was kept at similar pressure conditions under vacuum in the cryostat at all temperatures. Pump radiation was collected into the PCA gap with a plano-convex lens, resulting spot fully covered the gap ( $50 \mu\text{m}$ ). To distinguish photoinduced currents from thermally excited ones, similar dark I-V curves were recorded for the unpumped antenna and subsequently subtracted from the photoconductivity curves. The dependence of the photocurrent in the QDPCA on pump wavelength is shown in Figure 5.

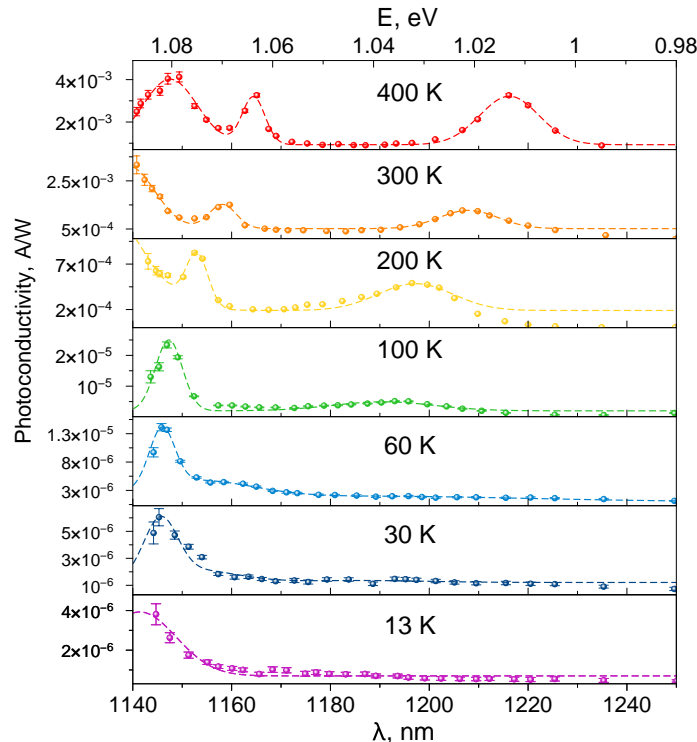


Figure 5. Photoconductivity spectra of QDPCA biased with 20V DC, at various temperatures. Dashed curves represent fitting with three (two for lower temperatures) gaussians, corresponding to GS and ES QD PCA photoconductivity peaks

All spectra reveal distinct peaks, clearly corresponding to the GS, ES1, and, for higher temperatures, when the energy falls within the laser operational range, the ES2. Photocurrent at other wavelengths pump is negligibly small. Peaks blueshift at lower temperatures follows the Varshni bandgap relation.

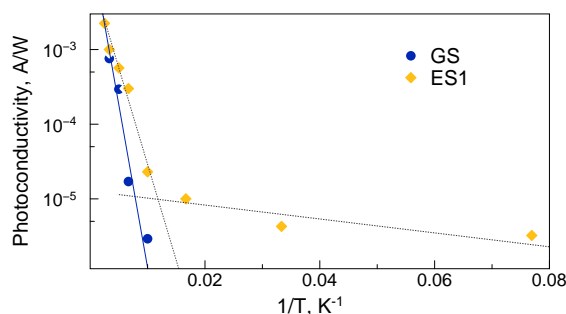


Figure 6. GS and ES1 Photoconductivity dependence on inverse temperature

The dependence of the GS and ES1 photocurrent on inverse temperature (Fig. 6), shows that GS amplitude can be fitted by an activation type curve with an activation energy of  $\sim 65$  meV. This value is greater than the energy separation between GS and ES1 ( $\sim 52$  meV at room temperature) and very close to GS and ES2 ( $\sim 68$  meV at room temperature). This indicates that thermal activation from the ground state to the excited states (particularly the upper one), with subsequent fast escape, plays a significant part in the carrier kinetics determining the photocurrent.<sup>33</sup>

At temperatures below 80 K, when thermal energy becomes insufficient for thermal activation, the GS photoconductivity is gradually vanishing, but the ES photoconductivity persists. This effect is explained by different dominating mechanisms of carrier extraction for these pumping conditions, and, also, as these mechanisms possess different characteristic times, vindicates the absence of THz generation under GS pump noticed in Section 3.1, due to slow thermal activation.

### 3.3 Efficient continuous wave terahertz generation in quantum dot photoconductive antennas under resonant pump

As the pulse THz generation and temperature dependent photoconductivity study suggest, QDPCA, if pumped at wavelengths corresponding to the QD ES, in theory, will have the ultrafast photocurrent. The technique that allows for the generation of continuously tunable coherent THz radiation is heterodyne mixing of two close optical wavelengths in a semiconductor surface. Thus, the only thing needed is the radiation with a double-wavelength pump at one of the wavelengths corresponding to the QD ES1 or ES2.

Instead of using a second tunable QD based laser, similar to the involved in the photocurrent study in Section 3.2, for the sake of compactness and higher wall plug efficiency, it was suggested to add a beamsplitter and a second diffraction grating into the laser cavity. Such configuration enables the independently tunable dual-wavelength operation. Moreover, joint use of similar QD structures in pump and PCA, demonstrates the potential of intracavity PCA placement in the future, resulting in ultra-compact, room-temperature, broadly-tunable THz laser source. Generated THz radiation was collected by a silicon lens. THz power was measured with a calibrated Goly cell, to enable its operation, a mechanical chopper was placed into one of the cavity shoulders. Such layout guarantees THz signal detection, as, regardless the chopper position, generated laser power is maintained by the current. The experimental setup is shown in Figure 7.

In order to obtain the THz signal, one wavelength of the pump laser was set to 1157.4 nm, which is just next to the photoconductance peak at 1157.3 nm, to ensure an efficient photocarrier generation. The second arm was tuned to achieve stable dual-colour laser operation with similar intensities for both wavelengths providing the difference frequencies of 0.74 THz and 0.83 THz, with total output power of double wavelength operation of 83 mW and 89 mW, correspondingly. The results of tunable THz generation in the QD PCA are presented in Figure 8.

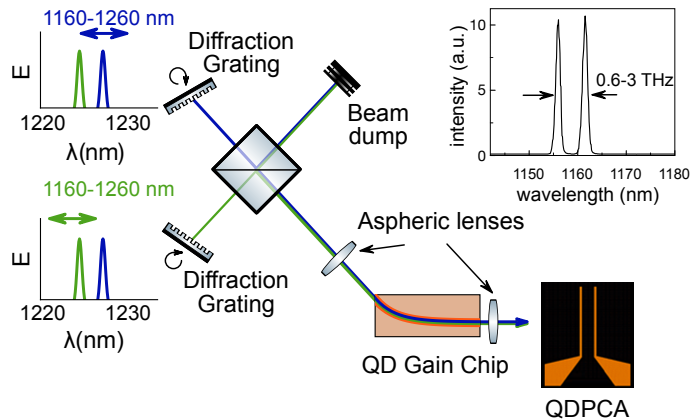


Figure 7. Setup for tunable CW THz generation in the QDPCA

Both THz signal bias trends can be easily fitted with second order curves, following the theoretical predictions. CW terahertz generation with a maximum output power of 0.25 nW was demonstrated at 0.74 THz.<sup>34</sup>

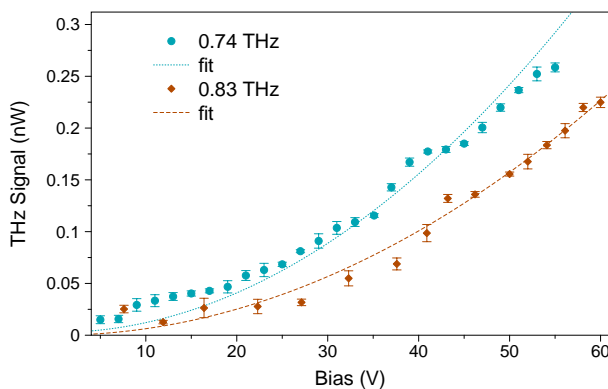


Figure 8. THz power dependences on bias applied to QDPCA. Lines show second order fits

#### 4. NON-RESONANT OPERATION OF QUANTUM DOT BASED PHOTOCONDUCTIVE ANTENNAS

As already mentioned above, photocarriers in QD substrates can be excited by not only the resonant pumping with the photon energy corresponding to the GS and ES of QDs, but also with photons with energy exceeding the GaAs bandgap  $\lambda \leq 870$  nm, due to carrier excitation in bulk GaAs containing the QDs, that play the key role being the sites of charge capture,<sup>29</sup> thereby shortening the lifetimes of the free carriers and allowing the use of such QD PCAs as both sources and detectors of pulsed and continuous THz radiation.

##### 4.1 Continuous wave terahertz radiation generation in quantum dot based photoconductive antennas under non-resonant pump

Figure 9 (a) shows one of the possible schemes for generating continuous THz radiation in an QD PCA.

The photomixer was pumped by two distributed feedback (DFB) AlGaAs semiconductor lasers with wavelengths of about 847 nm and 850 nm, electrically pumped with a current of 80 mA. The laser radiation was focused and coupled into an optical fiber. Laser wavelengths can be tuned in the range of about 0.66 nm by

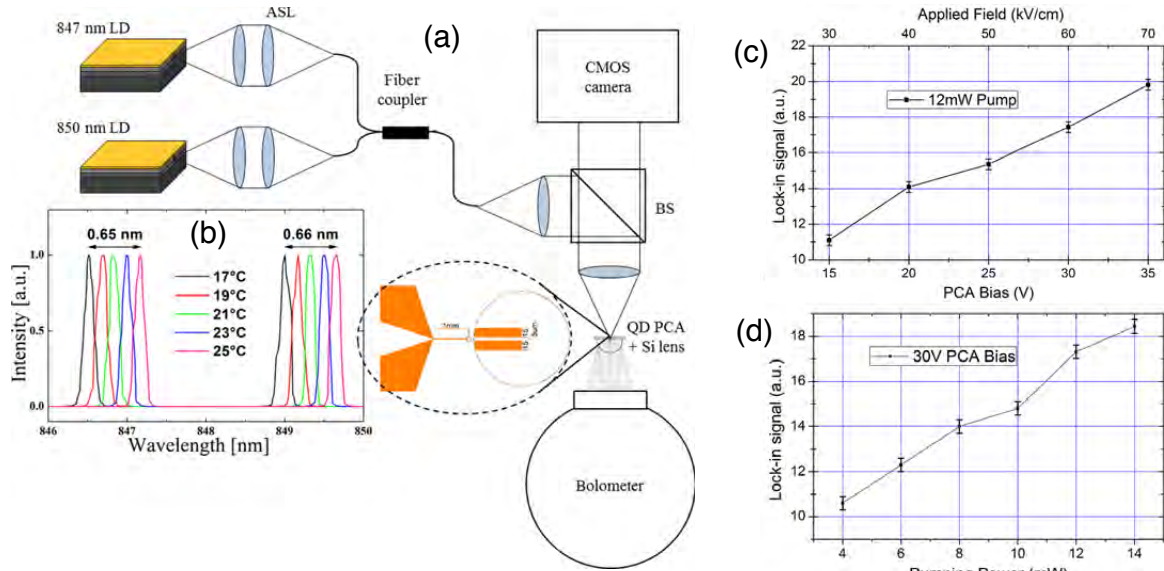


Figure 9. Experimental setup (a), and (b) the range of pumping wavelengths achievable by temperature tuning. ASL—aspherical lenses; BS—beam-splitting cube; and QD PCA. Dependence of the power of continuous THz radiation in a CT photomixer on the voltage at the electrodes (c), and the pumping power (d). Reproduced with permission from <sup>19</sup> © AIP

changing the laser operating temperature from 17°C to 25°C. This allows for tuning the difference frequency between 0.76 THz and 1.31 THz (Fig. 9 (b)). Typical spectral bandwidth of each laser was less than 0.2 nm. At 25°C, lasers yielded up to 100 mW power. The THz signal was registered using a liquid helium cooled germanium bolometer, synchronously amplified at the modulation frequency of the voltage supplied to the photomixer. A mesh bandpass filter with a transmission range of 0.6–10 THz was installed on the input window of the bolometer. It was shown that the bolometer signal increased repeatably as the bias at the PCA increased from 15 V to 35 V (Fig. 9 (c)), and as the optical pump power increased from 4 mW to 14 mW (Fig. 9 (d)). The results shown in the plots correspond to the peak difference frequency of the optical pump of 1.04 THz.<sup>19</sup>

#### 4.2 Generation of pulsed THz radiation in quantum dot based photoconductive antennas under non-resonant pump

When pumping a QD PCA using a Ti:Sapphire laser that operates at wavelengths short enough to excite the bulk GaAs barrier layers, optical-to-THz signal conversion takes place in the whole volume of the substrate. THz signal dependence on pump power is superlinear (Figure 10 (a)), saturation does not occur until pump power of at least 350 mW.

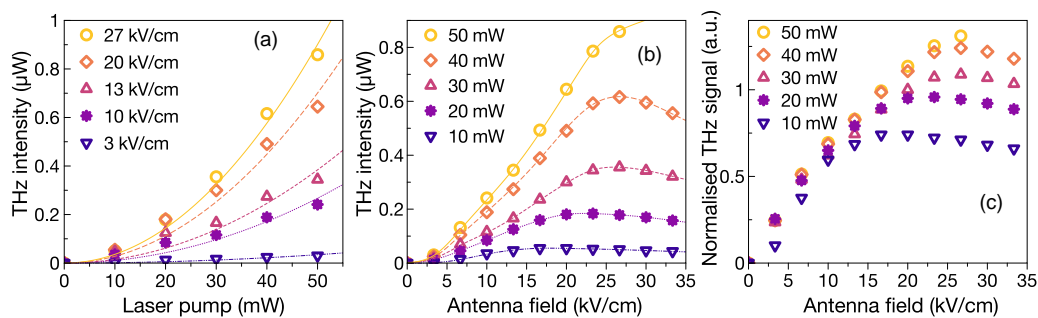


Figure 10. THz generation from a 25 layer QD PCA pumped using a fs Ti:Sapphire laser: (a) THz power versus laser pump power, (b) THz power at different fields applied to antenna. (c) THz signal normalised to the pump power

THz signal output power with increasing electric field applied to the PCA shows typical quadratic increase. However, at a certain value of antenna gap electric field strength, the THz signal starts to decrease. Interestingly, the point of signal saturation with respect to electric field strength appears to depend on the optical pump power, which is evident in Figure 10 (b).

After normalising the curves to the optical power, all points fall into a single dependence (Figure 10 (c)), with signal reduction occurring at lower fields applied under lower pump powers. This effect of electron velocity overshoot is the additional proof of fast electron trapping by QDs.<sup>29</sup>

Conventional LT-GaAs-based antennas with a similar electrode structure to the one used in this work allow a maximum laser pump power of up to around 50 mW. QD-based devices tolerate much greater input intensity and respond superlinearly not only at lower pump powers (Figure 10 (a)), but also at intensities ten times greater than the breakdown threshold of a bulk LT-GaAs device. The results of time-domain QDPCA characterisation are shown in Figure 11.

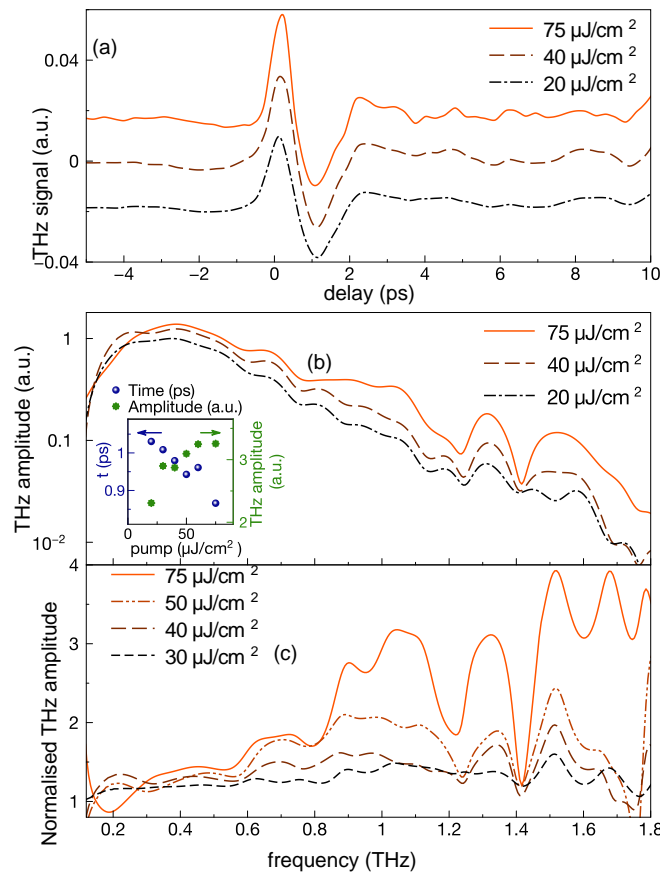


Figure 11. THz signal generated in the QD PCA pumped with a Ti:Sapphire laser. (a) Time-domain profile of the main pulse at different pump powers, signals are shifted for readability, (b) its corresponding amplitude spectra and (c) amplitude spectra normalised to one obtained at  $20 \mu\text{J}/\text{cm}^2$ . Insets show the antenna design ( $50 \mu\text{m}$  gap stripline (a)) and dependence of THz pulse duration and amplitude on pump energy density (b)

When changing the pump power within relatively low fluence limits, only the amplitude of the THz pulse is changed and, spectrum remains unchanged. However, at higher pump powers, not only does the amplitude of the pulse increase, but the pulsewidth also decreases in time (Figure 11 (a)). Trends for the points of THz pulse maximum amplitude and peak-to-peak duration are plotted in the inset of Figure 11 (b), and pulse shortening is clearly seen as well as pulse amplitude growth. Inherently, the corresponding spectra reveal inhomogeneous enhancement, higher frequency range of the signal rising more than the lower at higher pump energy densities

(Figure 11 (c)). To understand, whether this broadening is explained by Coulomb screening similarly to LT-GaAs<sup>35</sup> or by carrier lifetime shortening in QD samples due to Auger processes,<sup>20</sup> the next experiment, described in Section 4.3 was set up.

### 4.3 Carrier capture into quantum dots and carrier lifetime shortening in quantum dot based QD substrates

To study carrier lifetimes, a time-resolved THz time-domain spectrometer (TRTS) was used,<sup>27</sup> and THz differential transmission of the QD substrate was measured at various pump powers shown in Figure 12 (a). Importantly, THz radiation, unlike IR probe, depends on the concentration of only the free carriers present in the GaAs wafer and InGaAs wetting layer (WL), but not the excited carriers captured into QDs, unlike time-resolved PL, or optical pump-probe measurements. Similarly, only the probed mobile electrons are responsible for the THz generation in the PCA. Thus, optical pump-THz probe spectroscopy is the optimal tool for studying the characteristic free carrier capture into QDs time, responsible for spectral width in pulse generation and the efficiency of CW THz generation.

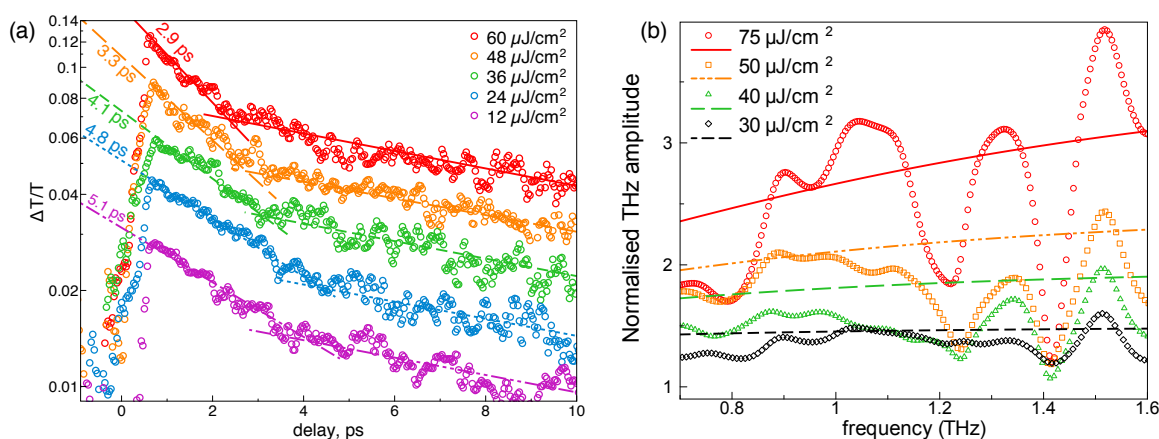


Figure 12. Relative transmission at maximum THz pulse amplitude through QD substrates. Exponential fits are plotted as a guide to the eye and reveal slower decay component, similar for all pump powers, and gradually shortening with pump power growth faster decay. Numbers show the exponent used for plotting the lines

From the plot in Figure 12 (a), it is clearly seen that the dynamics of the differential transmission curves is composed of two processes with different decay times, that correspond to faster carrier capture into QDs and slower recombination in the bulk GaAs. To illustrate this more clearly, slopes with independent single exponential fits, are shown. Faster component reduces at higher pumps.

To understand, whether this carrier lifetime shortening can be a reason for spectral broadening or not, a simulation of the photocurrent in the PCA using a laser pump dependent carrier lifetimes derived from the fits was performed. Carrier screening effect was omitted from the model, to discriminate the impact of lifetime shortening. After applying a Fourier transform to time dependent THz field, the resulting spectra are normalised to one at 20  $\mu\text{J}/\text{cm}^2$ , to correspond to the conditions used in the experiment. This comparison between simulation and experimental data is presented in Fig. 12 (b). Just as in experiment, at lower pump powers, the normalised spectra are quite flat, meaning that only the overall amplitude, but not the energy distribution within the spectrum depends on the pump power. On the other hand, for the highest pump power at 75  $\mu\text{J}/\text{cm}^2$ , the normalised spectrum reveals a clear slope that represents an uneven spectral intensity growth, and pretty much follows the experimental trend.

Thus, the trend of spectral broadening of the generated THz signal under higher pump powers experimentally observed is fully explained by the spectra, simulated with corresponding input pump powers and carrier lifetimes measured corresponding to that powers, without any carrier screening taken into account. Sharp features in the experimental curves originate from experimental conditions, such as water vapour absorption in the THz path, minor imperfections in alignment, or the impact of the antenna detector. The simulation does not take into

account all the aforementioned effects, hence the simulated curves look more smooth, while clearly repeating the general trend<sup>27</sup>

## 5. OUTLOOK

The inclusion of multiple bandgap-engineered semiconductor materials and quantum-confined structures enables additional pump absorption energy ranges and ultrafast charge carrier dynamics, different to those of bulk semiconductors, which is important for the optimisation of pump-PCA interaction and may be particularly crucial in the generation of continuous wave THz radiation. It is expected that a more tailored QD layer configuration could enhance the carrier capture and interaction rate and hence the signal conversion process. Preliminary results obtained with these first batches of samples have given a better insight into what exactly should be changed in the QD substrate structure to yield higher THz output in pulsed and CW regimes. Namely, for resonant pumps, pump laser wavelengths should coincide with QD excited state energies only. Moreover, it is necessary to rise the dot density on the substrates to shorten the free mean path and thus lower the lifetime. Low-defect absorption layers provide higher thermal conductivity and hence better pump power tolerance. Tunability of the photonic energies of QD LD output signals together with the versatile bandgap-engineering offered by QD-based PC materials, could allow the development of highly configurable, ultrafast optoelectronic systems. Both the LDs and the PCAs such as those used in this work may potentially be fabricated on the same epitaxial semiconductor wafer thus leading to fully integrated QD-based THz device. Apart from the listed measures, attention should be paid to modern nanophotonics solutions, like optical nanoantennas and metasurfaces that can be used to concentrate pump intensity into the QD surface layer.<sup>36–38</sup>

The low concentration of defects in QD substrates provides increased thermal conductivity and, therefore, allows the use of more powerful pumping lasers. Tunability of semiconductor QD lasers and the ability to set the absorption lines of substrates with the growth of CT materials allow the development of configurable, ultra-fast optoelectronic systems.

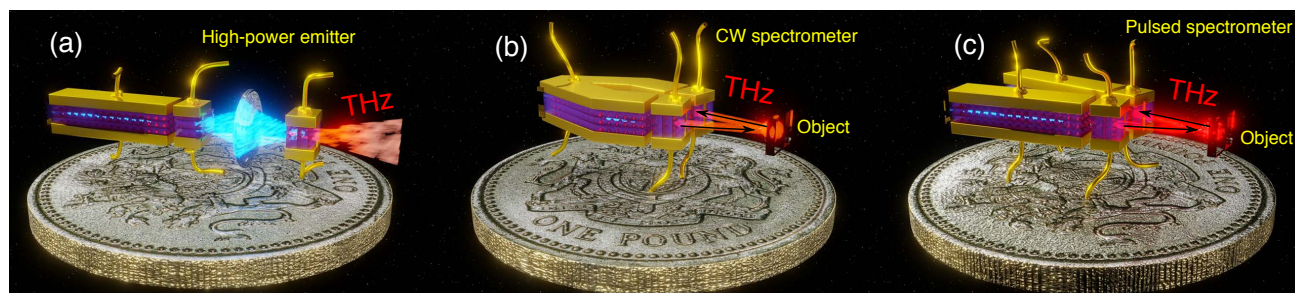


Figure 13. An artist's view of prospective compact QD laser based setups. (a) - VECSEL high-power system, (b) - CW spectrometer system, (c) - pulsed spectrometer system.

The tolerance to pumping power allows us to propose the possibility of placing such QD PCA directly in the resonator of a semiconductor laser, such as optically or electrically pumped Vertical External Cavity Surface Emitting Laser (VECSEL)<sup>12,39</sup> (Figure 13 (a)) and even grown on the same epitaxial semiconductor plate, eventually leading to the creation of fully integrated THz systems based on QD (Figure 13 (b, c)).

Further research into QD engineering has a very high potential to enable all-semiconductor-element-based, efficient, room-temperature operating THz transceivers with turn-key operation in an ultracompact housing.

## 6. CONCLUSION

In this contribution, we reviewed most recent achievements in THz generation with QD based PCAs including i) Generation and detection of pulsed terahertz radiation by InAs/GaAs QD based PCAs under pump radiation with photon energy below the gallium arsenide bandgap observed only at resonant pumping with energy corresponding to the QD excited states; ii) The absence of pulsed terahertz radiation generation in InAs/GaAs QD based PCAs, resonantly pumped at the QD ground state energy caused by the mechanism of excited carriers extraction from the QDs, which is different from extraction upon pumping into QD excited state; iii) Tunable continuous wave

terahertz radiation generation in InAs/GaAs QD based PCAs under resonant pump with photons corresponding to the QD excited state energy; iv) Spectral broadening of the generated pulsed terahertz radiation by non-resonantly pumped InAs/GaAs QD based PCAs at elevated pump powers caused by the reduction of free carriers lifetime; v) Five-fold boost at frequencies around 1 terahertz and more than two-fold increase in the overall generated terahertz radiation power by the silver spheroid nano-antennas in the gap of the PCA.

Developed InAs/GaAs QD based PCAs enabled the generation of THz radiation under the pump wavelengths generated by compact semiconductor lasers. In the process of development, the properties of the proposed substrates, such as photoconductivity and free carrier lifetimes, were studied in detail. The obtained results can be used to optimise the parameters of the substrates necessary for even more efficient conversion of the optical pump power into the radiated energy of the THz band. The proposed method for optimising the efficiency of silver nano-antennas can be applied not only to THz targets, but also in other areas requiring increased concentration of the electromagnetic field in the surface layer.

## ACKNOWLEDGMENTS

The authors thank D. Livshits from Innolume GmbH and Edmund Clark of the EPSRC National Centre for III-V Technologies, Sheffield, UK for QD samples growth and Richard Beanland from Integrity Scientific Ltd. for TEM image of a quantum dot. Also, we acknowledge Dr. Ross Leyman, for pioneering these experiments. This work was supported in part by EPSRC [Grant No EP/H015795/1] and FP7 IAPP TERA [project No 285974], and RFBR [Grants No. 18-07-01492 A and 16-07-01166 A]. Sample growth was funded by the NEXPRESSO program. A.G. thanks Magicplot LLC for providing a copy of MagicPlot Pro plotting and fitting software; and Vsevolod Gorodetsky for the assistance with illustrations.

## REFERENCES

- [1] Glagolewa-Arkadiewa, A., "Short Electromagnetic Waves of Wave-length up to 82 Microns," *Nature* **113**(2844), 640–640 (1924).
- [2] Williams, G. P., "Filling the THz gap—high power sources and applications," *Reports Prog. Phys.* **69**(2), 301–326 (2006).
- [3] Bradley, C., "Gain and frequency characteristics of a 20 mW C.W. water vapour laser oscillating at 118.6 microm," *Infrared Phys.* **12**(4), 287–299 (1972).
- [4] Jepsen, P., Cooke, D., and Koch, M., "Terahertz spectroscopy and imaging - Modern techniques and applications," *Laser Photon. Rev.* **5**(1), 124–166 (2011).
- [5] Knyazev, B. A., Kulipanov, G. N., and Vinokurov, N. A., "Novosibirsk terahertz free electron laser: instrumentation development and experimental achievements," *Meas. Sci. Technol.* **21**(5), 054017 (2010).
- [6] Valavanis, A., Zhu, J., Freeman, J., Li, L., Chen, L., Davies, A., Linfield, E., and Dean, P., "Terahertz quantum cascade lasers with >1 W output powers," *Electron. Lett.* **50**(4), 309–311 (2014).
- [7] Dhillon et al., S. S., "The 2017 terahertz science and technology roadmap," *J. Phys. D. Appl. Phys.* **50**(4), 043001 (2017).
- [8] Baba, R., Jacobs, K. J., Stevens, B. J., Harrison, B. A., Watt, A. P., Mukai, T., and Hogg, R. A., "Resonant Tunnelling Diodes for next generation THz systems," in [2018 Br. Irish Conf. Opt. Photonics, BICOP 2018 - Proc.], (December 2018), 1–4, IEEE (2019).
- [9] Belkin, M. A. and Capasso, F., "New frontiers in quantum cascade lasers: high performance room temperature terahertz sources," *Phys. Scr.* **90**(11), 118002 (2015).
- [10] Xie, X., Dai, J., and Zhang, X.-C., "Coherent Control of THz Wave Generation in Ambient Air," *Phys. Rev. Lett.* **96**(7), 075005 (2006).
- [11] Castro-Camus, E. and Alfaro, M., "Photoconductive devices for terahertz pulsed spectroscopy: a review [Invited]," *Photonics Res.* **4**(3), A36 (2016).
- [12] Gorodetsky, A., Bazieva, N., and Rafailov, E. U., "Quantum-dot based ultrafast photoconductive antennae for efficient THz radiation," in [SPIE Proceedings], **9737**, 97370C (2016).
- [13] Arakawa, Y. and Sakaki, H., "Multidimensional quantum well laser and temperature dependence of its threshold current," *Appl. Phys. Lett.* **40**(11), 939–941 (1982).

- [14] Ekimov, A., Efros, A., and Onushchenko, A., “Quantum size effect in semiconductor microcrystals,” *Solid State Commun.* **56**(11), 921–924 (1985).
- [15] Auston, D. H., Cheung, K. P., and Smith, P. R., “Picosecond photoconducting Hertzian dipoles,” *Appl. Phys. Lett.* **45**(3), 284–286 (1984).
- [16] Reed, M. A., “Quantum Dots,” *Sci. Am.* **268**(1), 118–123 (1993).
- [17] Kadow, C., Jackson, A. W., Gossard, A. C., Bowers, J. E., Matsuura, S., and Blake, G. A., “Self-assembled ErAs islands in GaAs for THz applications,” *Phys. E Low-dimensional Syst. Nanostructures* **7**(1-2), 97–100 (2000).
- [18] Estacio, E., Pham, M. H., Takatori, S., Cadatal-Raduban, M., Nakazato, T., Shimizu, T., Sarukura, N., Somintac, A., Defensor, M., Awitan, F. C. B., Jaculbia, R. B., Salvador, A., and Garcia, A., “Strong enhancement of terahertz emission from GaAs in InAs/GaAs quantum dot structures,” *Appl. Phys. Lett.* **94**(23), 232104 (2009).
- [19] Kruczek, T., Leyman, R., Carnegie, D., Bazieva, N., Erbert, G., Schulz, S., Reardon, C., Reynolds, S., and Rafailov, E. U., “Continuous wave terahertz radiation from an InAs/GaAs quantum-dot photomixer device,” *Appl. Phys. Lett.* **101**(8), 081114 (2012).
- [20] Rafailov, E., White, S., Lagatsky, A., Miller, A., Sibbett, W., Livshits, D., Zhukov, A., and Ustinov, V., “Fast Quantum-Dot Saturable Absorber for Passive Mode-Locking of Solid-State Lasers,” *IEEE Photonics Technol. Lett.* **16**(11), 2439–2441 (2004).
- [21] Liu, H.-Y., Meng, Z.-M., Dai, Q.-F., Wu, L.-J., Guo, Q., Hu, W., Liu, S.-H., Lan, S., and Yang, T., “Ultrafast carrier dynamics in undoped and p-doped InAs/GaAs quantum dots characterized by pump-probe reflection measurements,” *J. Appl. Phys.* **103**(8), 083121 (2008).
- [22] Ponomarev, D. S., Gorodetsky, A., Yachmenev, A. E., Pushkarev, S. S., Khabibullin, R. A., Grekhov, M. M., Zaytsev, K. I., Khusyainov, D. I., Buryakov, A. M., and Mishina, E. D., “Enhanced terahertz emission from strain-induced InGaAs/InAlAs superlattices,” *J. Appl. Phys.* **125**(15), 151605 (2019).
- [23] Beard, M. C., Turner, G. M., and Schmuttenmaer, C. a., “Subpicosecond carrier dynamics in low-temperature grown GaAs as measured by time-resolved terahertz spectroscopy,” *J. Appl. Phys.* **90**(12), 5915–5923 (2001).
- [24] Cooke, D. G., Hegmann, F. A., Young, E. C., and Tiedje, T., “Electron mobility in dilute GaAs bismide and nitride alloys measured by time-resolved terahertz spectroscopy,” *Appl. Phys. Lett.* **89**(12), 122103 (2006).
- [25] Bertulis, K., Krotkus, A., Aleksejenko, G., Pačebutas, V., Adomavičius, R., Molis, G., and Marcinkevičius, S., “GaBiAs: A material for optoelectronic terahertz devices,” *Appl. Phys. Lett.* **88**(20), 201112 (2006).
- [26] Oh, S. J., Kang, C., Maeng, I., Son, J.-H., Cho, N. K., Song, J. D., Choi, W. J., Cho, W.-J., and Lee, J. I., “Measurement of carrier concentration captured by InAs/GaAs quantum dots using terahertz time-domain spectroscopy,” *Appl. Phys. Lett.* **90**(13), 131906 (2007).
- [27] Gorodetsky, A., Bazieva, N., and Rafailov, E. U., “Pump dependent carrier lifetimes in InAs/GaAs quantum dot photoconductive terahertz antenna structures,” *J. Appl. Phys.* **125**(15), 151606 (2019).
- [28] Rafailov, E. U., Cataluna, M. A., and Sibbett, W., “Mode-locked quantum-dot lasers,” *Nat. Photonics* **1**(7), 395–401 (2007).
- [29] Leyman, R. R., Gorodetsky, A., Bazieva, N., Molis, G., Krotkus, A., Clarke, E., and Rafailov, E. U., “Quantum dot materials for terahertz generation applications,” *Laser Photon. Rev.* **10**(5), 772–779 (2016).
- [30] Mingardi, A., Zhang, W.-D., Brown, E. R., Feldman, A. D., Harvey, T. E., and Mirin, R. P., “High power generation of THz from 1550-nm photoconductive emitters,” *Opt. Express* **26**(11), 14472 (2018).
- [31] Zhang, W., Brown, E. R., Mingardi, A., Mirin, R. P., Jahed, N., and Saeedkia, D., “THz Superradiance from a GaAs: ErAs Quantum Dot Array at Room Temperature,” *Appl. Sci.* **9**(15), 3014 (2019).
- [32] Yukalov, V. I. and Yukalova, E. P., “Dynamics of quantum dot superradiance,” *Phys. Rev. B* **81**(7), 075308 (2010).
- [33] Gorodetsky, A., Yadav, A., Avrutin, E., Fedorova, K. A., and Rafailov, E. U., “Photoelectric Properties of InAs/GaAs Quantum Dot Photoconductive Antenna Wafers,” *IEEE J. Sel. Top. Quantum Electron.* **24**(2), 1–5 (2018).
- [34] Fedorova, K. A., Gorodetsky, A., and Rafailov, E. U., “Compact All-Quantum-Dot-Based Tunable THz Laser Source,” *IEEE J. Sel. Top. Quantum Electron.* **23**(4), 1–5 (2017).

- [35] Pedersen, J. E., Lyssenko, V. G., Hvam, J. M., Jepsen, P. U., Keiding, S. R., So/rensen, C. B., and Lindelof, P. E., "Ultrafast local field dynamics in photoconductive THz antennas," *Appl. Phys. Lett.* **62**(11), 1265–1267 (1993).
- [36] Lepeshov, S., Gorodetsky, A., Krasnok, A., Rafailov, E., and Belov, P., "Enhancement of terahertz photoconductive antenna operation by optical nanoantennas," *Laser Photon. Rev.* **11**(1), 1600199 (2017).
- [37] Lepeshov, S., Gorodetsky, A., Krasnok, A., Toropov, N., Vartanyan, T. A., Belov, P., Alú, A., and Rafailov, E. U., "Boosting Terahertz Photoconductive Antenna Performance with Optimised Plasmonic Nanostructures," *Sci. Rep.* **8**(1), 6624 (2018).
- [38] Gric, T., Gorodetsky, A., Trofimov, A., and Rafailov, E., "Tunable Plasmonic Properties and Absorption Enhancement in Terahertz Photoconductive Antenna Based on Optimized Plasmonic Nanostructures," *J. Infrared, Millimeter, Terahertz Waves* **39**(10), 1028–1038 (2018).
- [39] Gorodetsky, A., Fedorova, K. A., Bazieva, N., and Rafailov, E. U., "Generating tunable terahertz radiation with a novel quantum dot photoconductive antenna," *SPIE Newsroom*, 2–4 (2016).